Electronic Supplementary Material (ESI) for Dalton Transactions

Electronic Supporting Information:

Encapsulation of trivalent phosphate anion within a rigidified π-stacked dimeric capsular assembly of tripodal receptor

*Sandeep Kumar Dey and Gopal Das**

Department of Chemistry, Indian Institute of Technology Guwahati, Assam, 781 03, India,.

Fax: +91-361-258-2349; Tel: +91-361-258-2313

E-mail: gdas@iitg.ernet.in

Experimental Section:

^{1}H and ^{13}C NMR spectra were recorded on a Varian FT-400 MHz spectrometer in DMSO- d_6 at 298 K. Chemical shifts for ^{1}H and ^{13}C NMR were reported in parts per million (ppm), calibrated to the residual solvent peak set, with coupling constants reported in Hertz (Hz). The IR spectra were recorded on a Perkin-Elmer-Spectrum One FT-IR spectrometer with KBr disks in the range 4000-450 cm^{-1}. All tetrabutylammonium (TBA) salts used were purchased from Sigma-Aldrich, USA and were used as received. Solvents used for the synthesis and crystallization experiments (THF and MeCN) were of HPLC grade and purchased from Spectrochem Ltd., India.

Synthesis of tris-(thiourea) receptor, L:

Tripodal thiourea-based receptor, **L** was synthesized by the reaction of tris(2-aminoethyl)amine with three equivalents of 4-nitrophenyl isothiocyanate in THF by stirring overnight at RT. After overnight stirring, solvents were removed under *vacuo* and the obtained solid product was washed with plenty methanol to remove the unreacted reagents. Finally, the product was filtered and dried under vacuum to yield yellow solid of **L** (Yield = 84%). The ligand has been characterized by NMR, FT-IR, ESI-MS and elemental analysis. Single crystals of **L** suitable for X-ray diffraction analysis were grown from DMF at RT.

^{1}H NMR titration experiments:

Binding constants were obtained by ^{1}H NMR (400 MHz) titrations of **L** with tetrabutylammonium salts of respective anions in DMSO-d_6 at 298 K. The initial concentration of corresponding receptor was 10 mM. Aliquots of anions were added from 50 mM stock solutions of anions (up to 1:3 or 1:5 host/guest stoichiometries). The residual solvent peak in DMSO-d_6 (2.50 ppm) was used as an internal reference, and each titration was performed with 10-15 measurements at room temperature.

Following equation was used to determine the K values:[1]

$$\Delta\delta = \{([A]_0 + [\mathbf{L}]_0 + 1/K) +/- (([A]_0 + [\mathbf{L}]_0 + 1/K)^2 - 4[\mathbf{L}]_0[A]_0)^{1/2}\}\Delta\delta_{max}/2[\mathbf{L}]_0$$

Table S1. Crystallographic details of data collection for receptor **L** and complexes **1** and **2.**

Parameters	**L•DMF**	**Complex 1**	**Complex 2**
formula	$C_{30}H_{37}N_{11}O_7S_3$	$C_{106}H_{174}N_{25}O_{16}PS_6$	$C_{45}H_{69}FN_{12}O_6S_3$
*M*r	759.92	2278.09	989.33
Lattice system	Triclinic	Triclinic	Triclinic
Space group	*P*-1	*P*-1	*P*-1
a/Å	9.3675(5)	13.5840(7)	13.0874(4)
b/Å	10.4400(6)	16.0821(8)	13.1320(4)
c/Å	19.5297(11)	28.9547(15)	35.7500(11)
α/°	94.671(4)	103.421(4)	79.965(2)
β/°	92.962(4)	93.523(4)	86.542(3)
γ/°	110.626(3)	92.808(4)	60.285(2)
V/Å^3	1774.95(18)	6128.0(6)	5252.1(3)
Z	2	2	4
D_c/g cm^{-1}	1.422	1.235	1.251
μ Mo K_α/mm^{-1}	0.271	0.194	0.201
2 theta	28.340	28.460	28.360
Total reflections	24704	92714	49038
Independent reflections	8599	29779	25528
Observed reflections	6935	24513	21878
Parameters refined	463	1401	1217
R_1; wR_2 (all data)	0.0890; 0.2071	0.0860; 0.2158	0.0875; 0.2076
GOF (F^2)	1.061	1.067	1.0061

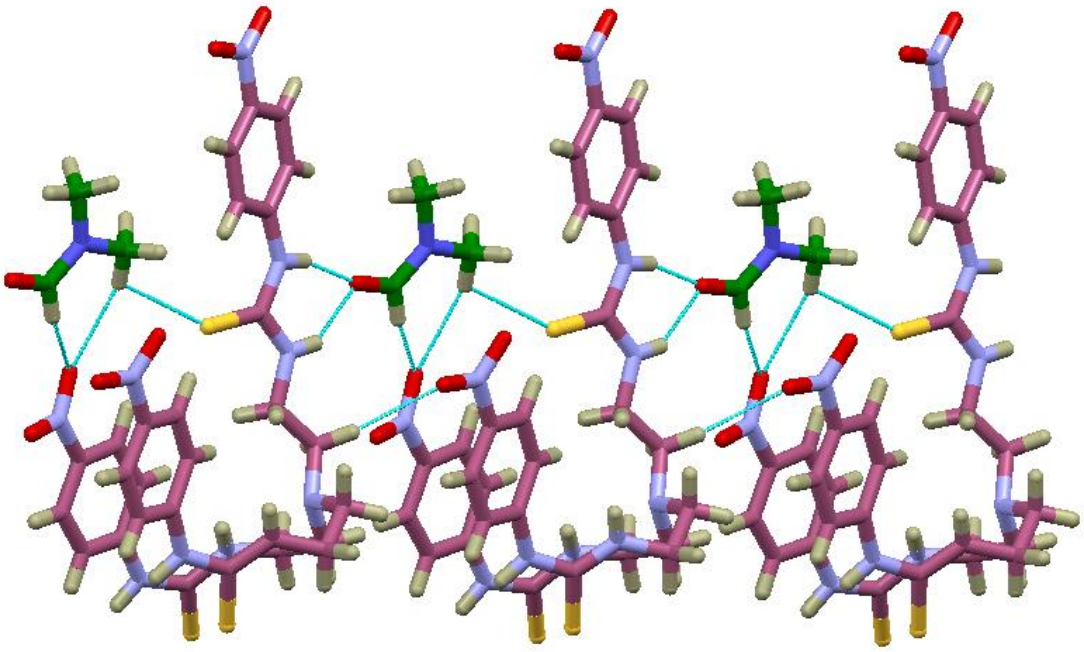

Figure S1. Ball and stick representation of crystal structure of **L•DMF** depicting the interactions (blue dotted lines) of the receptor molecules with lattice DMF (green).

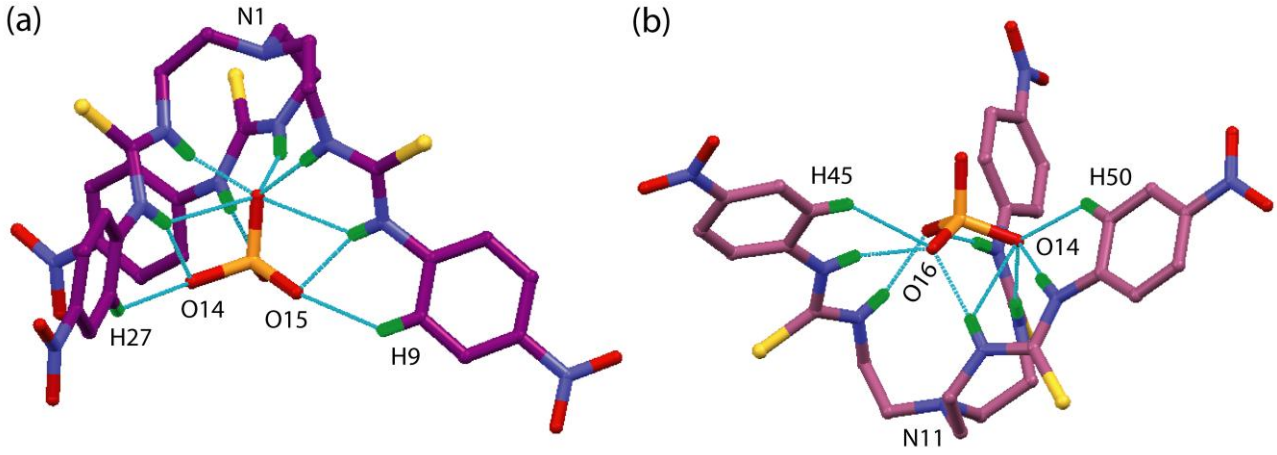

Figure S2. Ball and stick representation of crystal structure of **1** depicting the interactions (blue dotted lines) of the –NH and aryl –CH protons with phosphate anion when the *d*(D•••A) is restricted to < 3.5 Å for H-bonding; (a) axial **L** coordinating to PO_4^{3-} and (b) facial **L** coordinating to PO_4^{3-}.

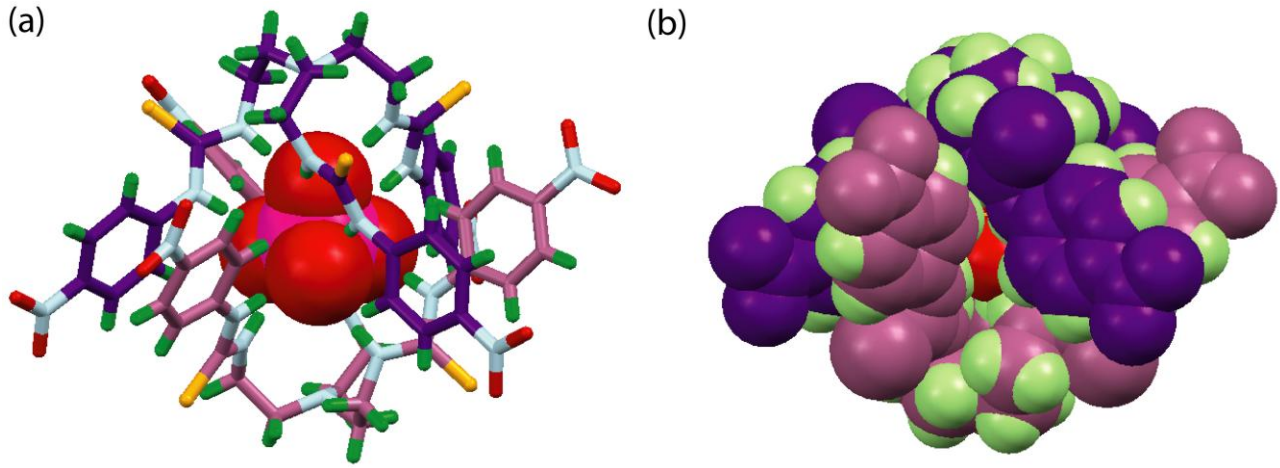

Figure S3. Spacefill representation depicting the full encapsulation of trivalent phosphate anion within the π-stacked dimeric cage of receptor **L**. Two symmetry independent molecules are shown in different colours and countercations are omitted for clarity of presentation.

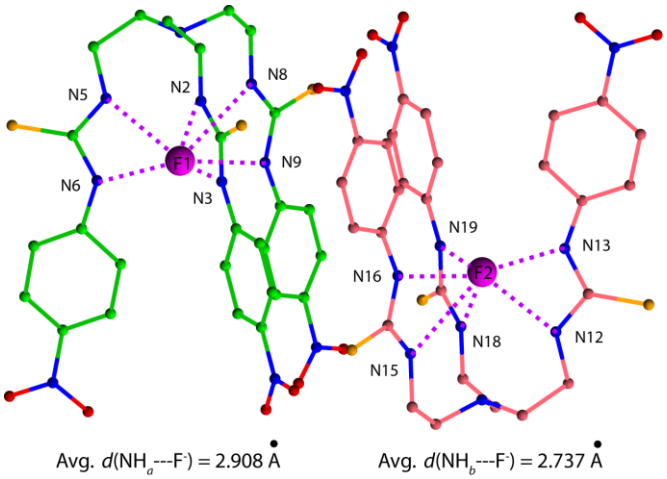

Figure S4. Ball and stick representation depicting the six H-bonding interactions of F^- within the tripodal cavity of two symmetry independent units of **L**. Countercations and solvent molecules are omitted for clarity of presentation.

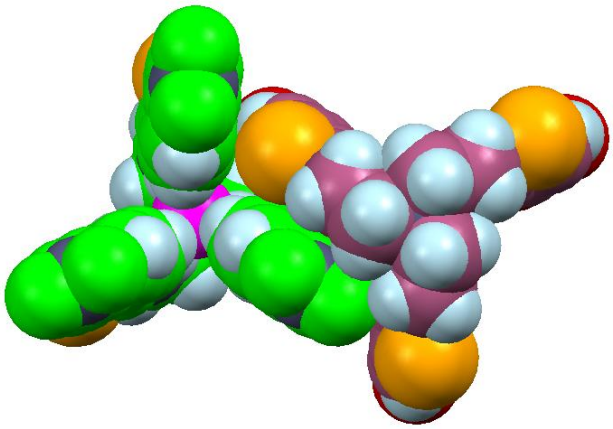

Figure S5. Spacefill representation depicting the encapsulation of fluoride anion within the tripodal scaffold of two symmetry independent **L** units assembled by C-H•••π and π•••π interactions.

Table S2. Hydrogen bonding interactions of PO_4^{-3} within the dimeric cage of **L** in complex **1.**

Complex **1**, 3TBA[2**L**(PO_4)]•2MeCN			
When *d*(D•••A) < 3.00 Å for H-bonding			
D-H••••O	*d*(H••••O)/Å	*d*(D••••O)/Å	<D-H••••O/^{o}
N2-H••••O13	1.92(2)	2.781(4)	178(2)
N5-H••••O13	1.93(3)	2.730(5)	154(3)
N8-H••••O13	1.90(2)	2.733(4)	161(3)
N9-H••••O14	2.05(2)	2.862(5)	156(3)
N12-H••••O14	2.06(3)	2.908(4)	166(2)
N19-H••••O14	1.86(2)	2.721(4)	170(2)
N3-H••••O15	1.97(2)	2.776(4)	153(2)
N13-H••••O15	1.89(3)	2.749(5)	174(2)
N15-H••••O15	1.96(2)	2.792(4)	162(2)
N6-H••••O16	2.02(3)	2.872(4)	167(3)
N16-H••••O16	2.00(2)	2.823(4)	158(3)
N18-H••••O16	2.01(2)	2.844(4)	160(2)
When *d*(D•••A) < 3.50 Å for H-bonding			
N3-H••••O13	2.69(2)	3.403(4)	141(2)
N9-H••••O13	2.71(3)	3.393(4)	137(3)
N18-H••••O14	2.71(3)	3.339(4)	131(2)
C27-H••••O14	2.62(3)	3.333(5)	133(3)
C50-H••••O14	2.56(2)	3.284(5)	134(3)
C9-H••••O15	2.54(2)	3.164(5)	124(3)
C45-H••••O16	2.69(3)	3.423(6)	135(4)

Table S3. Hydrogen bonding interactions of F^- with receptor **L** in complex **2.**

Complex **2**, TBA[**L**(F)]•MeCN			
D-H••••O	*d*(H••••O)/Å	*d*(D••••O)/Å	<D-H••••O/^{o}
N2-H••••F1	2.15(2)	2.910(4)	146(2)
N3-H••••F1	1.88(2)	2.729(4)	166(2)
N5-H••••F1	2.19(2)	2.937(5)	145(3)
N6-H••••F1	1.88(3)	2.730(5)	169(3)
N8-H••••F1	2.10(2)	2.874(4)	148(3)
N9-H••••F1	1.91(2)	2.749(3)	163(3)
N12-H••••F2	2.12(2)	2.882(4)	147(2)
N13-H••••F2	1.90(3)	2.743(5)	164(2)
N15-H••••F2	2.21(2)	2.956(4)	145(2)
N16-H••••F2	1.88(2)	2.731(3)	168(2)
N18-H••••F2	2.13(2)	2.894(4)	148(3)
N19-H••••F2	1.90(2)	2.744(5)	166(3)

Characterization of receptor L:

m.p. = 225-230 ^{o}C; ^{1}H-NMR (400 MHz, DMSO-d_6) δ 2.814 (s, 6H, -NCH_2), 3.660 (s, 6H, -NCH_2CH_2), 7.764-7.787 (d, 6H, ArH), 8.127-8.149 (d, 6H, ArH), 8.174 (s, 3H, -CH_2NH), 10.205 (s, 3H, Ar-NH); ^{13}C NMR (100 MHz, DMSO-d_6): δ 41.90 (×3C, -NCH_2), 51.62 (×3C, -NCH_2CH_2), 120.38 (×6C, ArH), 124.52 (×6C, ArH), 141.78 (×3C, ArH), 146.25 (×3C, ArH), 179.95 (×3C, C=S); ESI-MS: *m/z* [**L**+H]$^{+}$ 687.1639; FT-IR (KBr, υ cm^{-1}): 715, 1112, 1334, 1510, 2927, 3339; Anal. Calcd for $C_{30}H_{37}N_{11}O_7S_3$: C, 47.22; H, 4.40; N, 20.39. Found: C, 47.34; H, 4.18; N, 19.87.

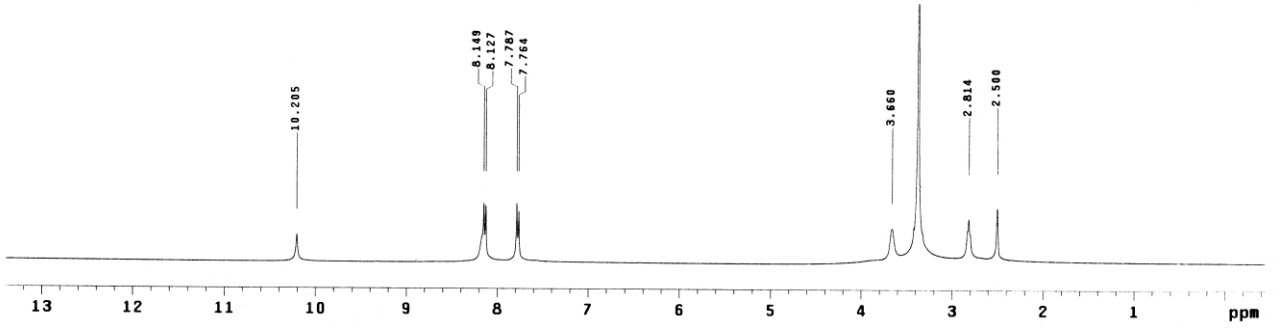

Figure S6. ^{1}H NMR spectrum of **L** in DMSO-d_6 at 298 K.

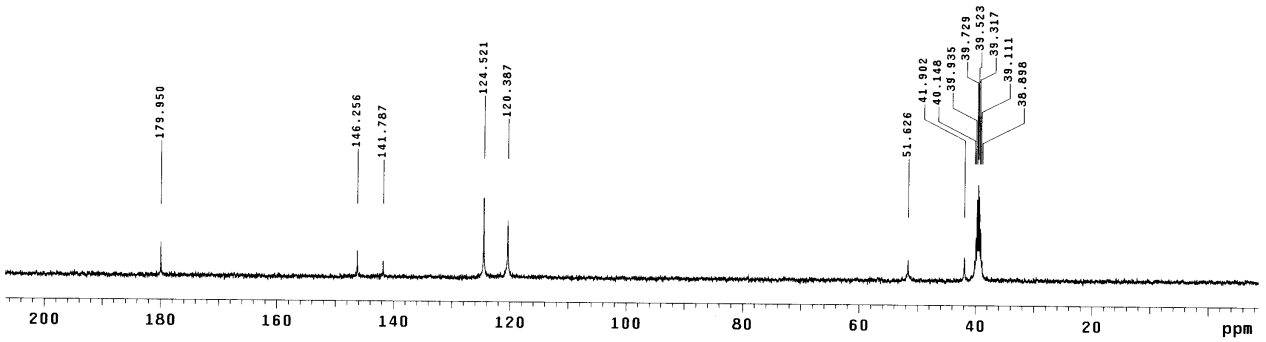

Figure S7. ^{13}C NMR spectrum of **L** in DMSO-d_6 at 298 K.

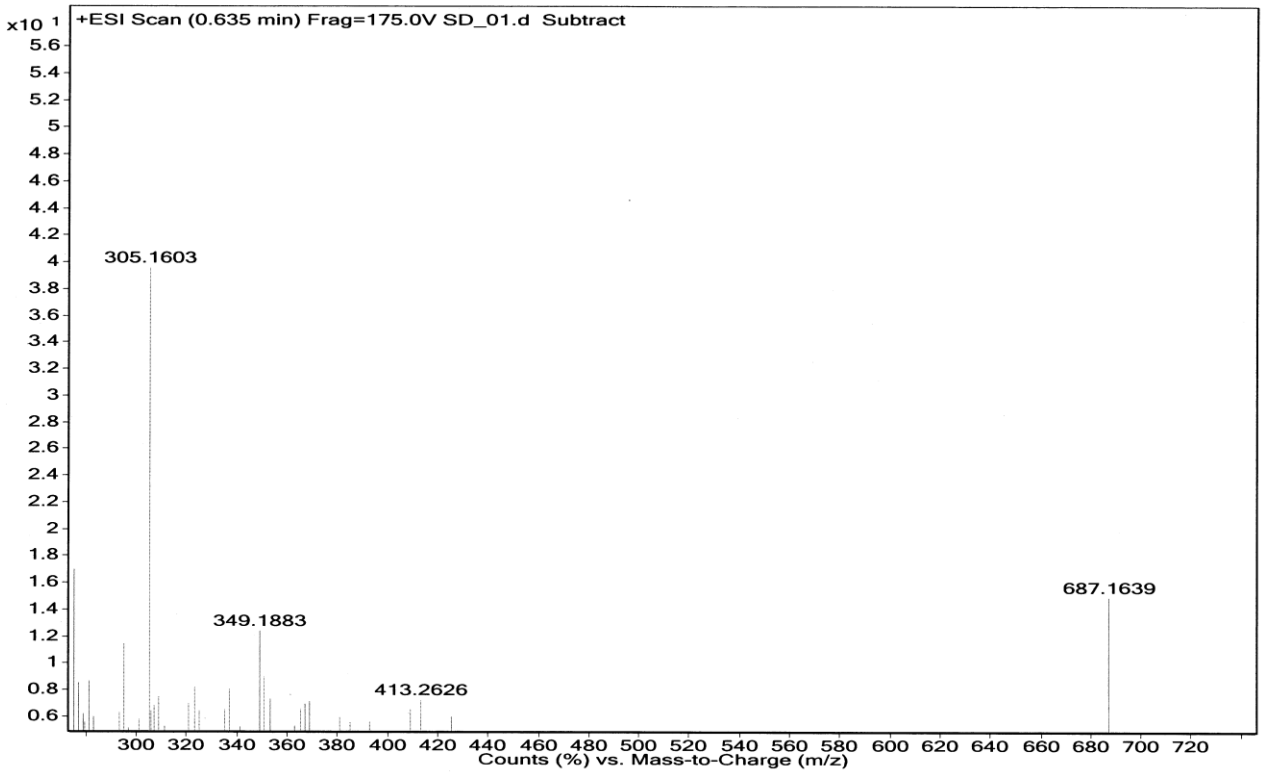

Figure S8. Positive ion mode ESI-mass spectrum of **L** in acetonitrile.

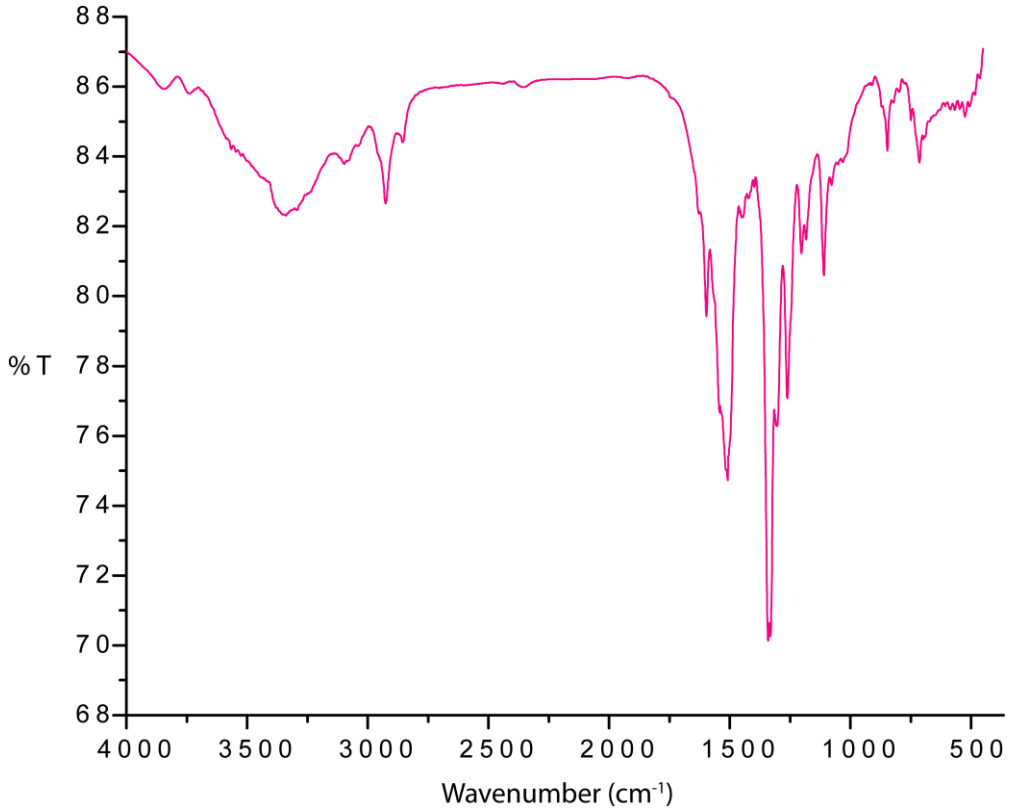

Figure S9. FT-IR spectrum of receptor **L** recorded in KBr pellet.

Characterization of phosphate complex, 1:

^{1}H-NMR (400 MHz, DMSO-d_6) δ 0.928-0.966 (t, -CH_3, TBA), 1.285-1.358 (q, -CH_2, TBA), 1.559-1.577 (t, -CH_2, TBA), 3.046-3.087 (t, -NCH_2, TBA), 1.933-1.959 (q, CH_3CN), 2.703 (s, 12H, -NCH_2), 3.507 (s, 12H, -NCH_2CH_2), 7.746-7.807 (q, ArH), 11.935 (s, 6H, -CH_2NH), 12.998 (s, 6H, Ar-NH); ^{13}C NMR (100 MHz, DMSO-d_6): δ 13.85 (×12C, -CH_3, TBA), 20.37 (×12C, -CH_2, TBA), 24.35 (×12C, -CH_2, TBA), 59.37 (×12C, -NCH_2, TBA), 44.30 (×6C, -NCH_2), 56.65 (×6C, -NCH_2CH_2), 121.17 (×12C, ArH), 124.33 (×12C, ArH), 141.82 (×6C, ArH), 149.85 (×6C, ArH), 181.73 (×6C, C=S); FT-IR (KBr, υ cm^{-1}): 1009, 1110, 1277, 1327, 1510, 1561, 2964, 3440.

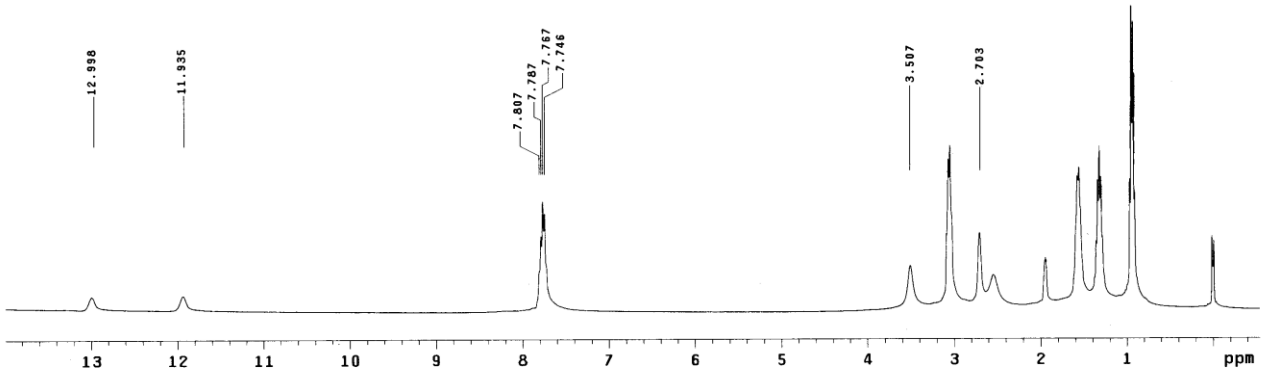

Figure S10. ^{1}H NMR spectrum of phosphate complex (**1**) in DMSO-d_6 at 298 K.

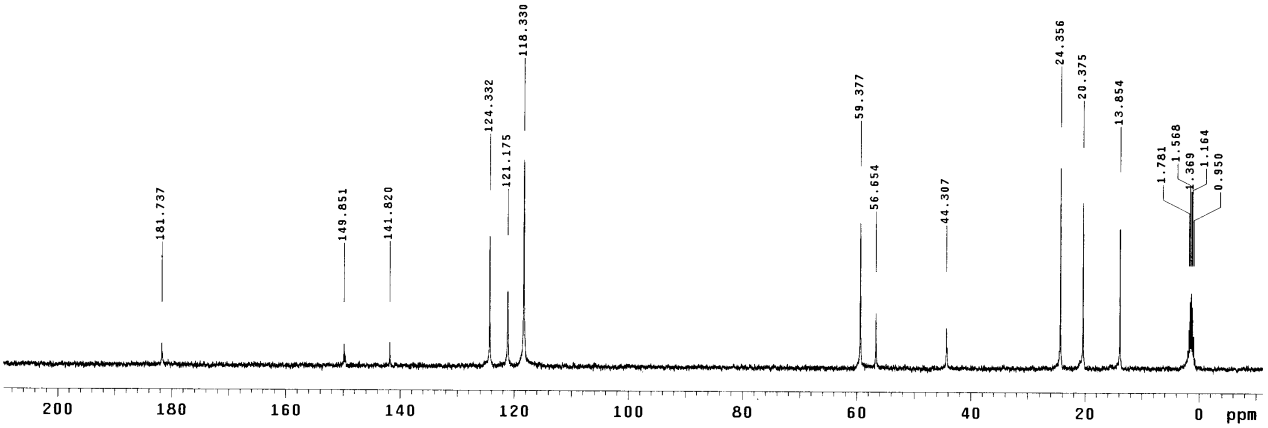

Figure S11. ^{13}C NMR spectrum of phosphate complex (**1**) in DMSO-d_6 at 298 K.

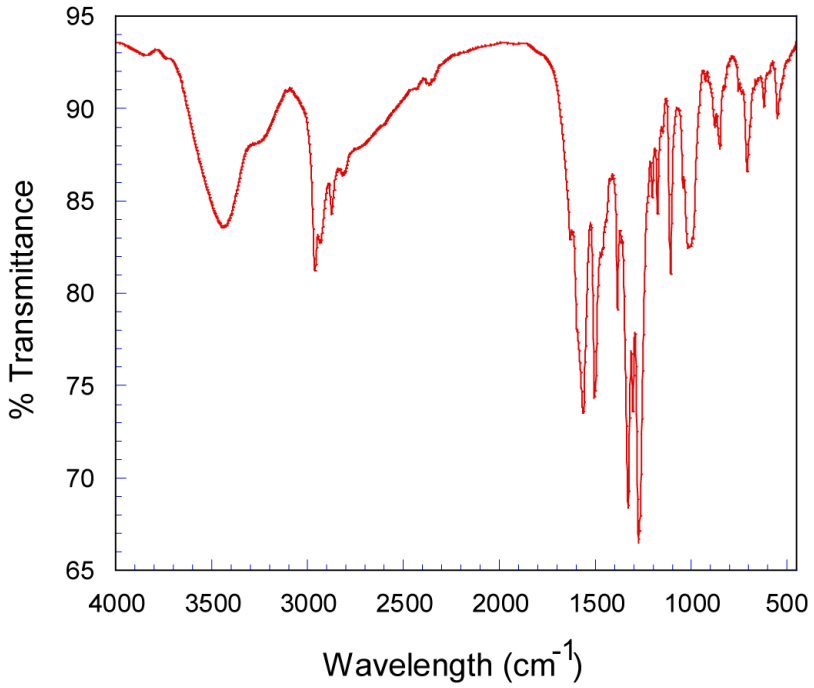

Figure S12. FT-IR spectrum of phosphate complex (**1**) recorded in KBr pellet.

Characterization of fluoride complex, 2:

^{1}H-NMR (400 MHz, DMSO-d_6) δ 0.915-0.951 (t, -CH_3, TBA), 1.282-1.335 (q, -CH_2, TBA), 1.563 (s, -CH_2, TBA), 3.131-3.171 (t, -NCH_2, TBA), 2.077 (s, CH_3CN), 2.707 (s, 6H, -NCH_2), 3.613 (s, 6H, -NCH_2CH_2), 7.947-7.968 (d, 6H, ArH), 8.090-8.112 (d, 6H, ArH), 9.035 (s, 3H, -CH_2NH), 11.915 (s, 3H, Ar-NH); ^{13}C NMR (100 MHz, DMSO-d_6): δ 13.03 (×4C, -CH_3, TBA), 19.57 (×4C, -CH_2, TBA), 23.54 (×4C, -CH_2, TBA), 58.59 (×4C, -NCH_2, TBA), 40.91 (×3C, -NCH_2), 51.24 (×3C, -NCH_2CH_2), 120.05 (×6C, ArH), 124.42 (×6C, ArH), 139.44 (×3C, ArH), 151.24 (×3C, ArH), 180.99 (×3C, C=S); FT-IR (KBr, υ cm^{-1}): 843, 1108, 1331, 1510, 1537, 2965, 3273.

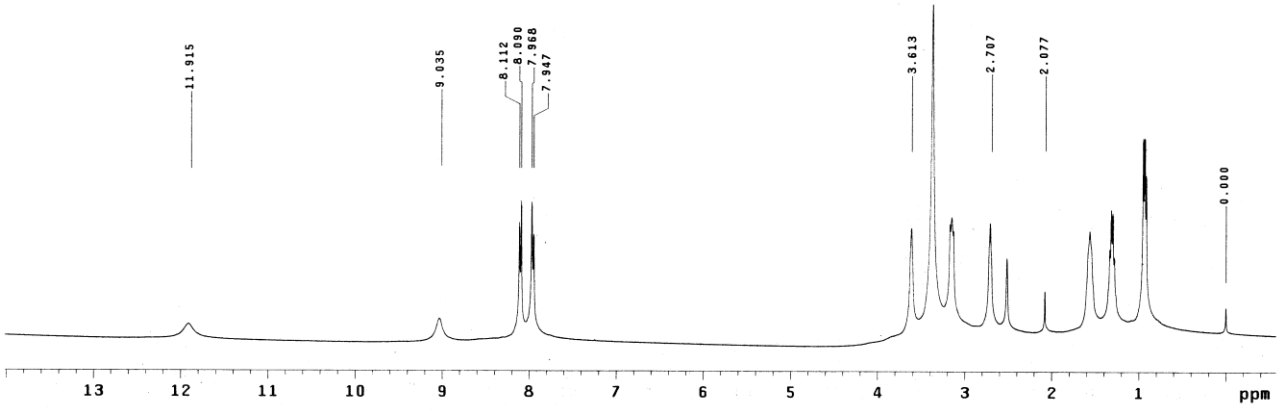

Figure S13. ^{1}H NMR spectrum of fluoride complex (**2**) in DMSO-d_6 at 298 K.

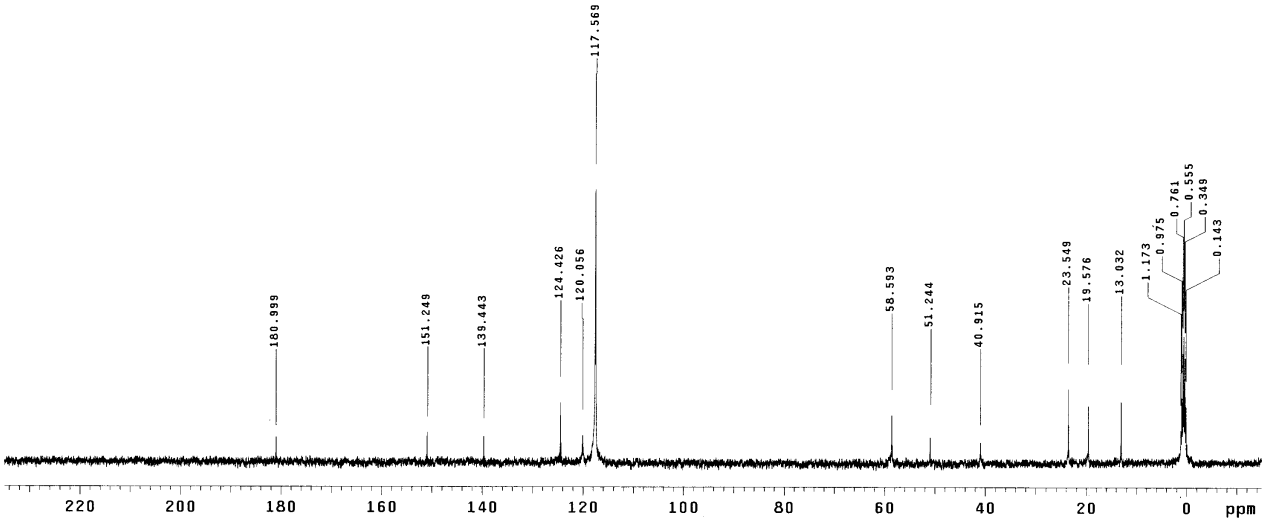

Figure S14. ^{13}C NMR spectrum of fluoride complex (**2**) in DMSO-d_6 at 298 K.

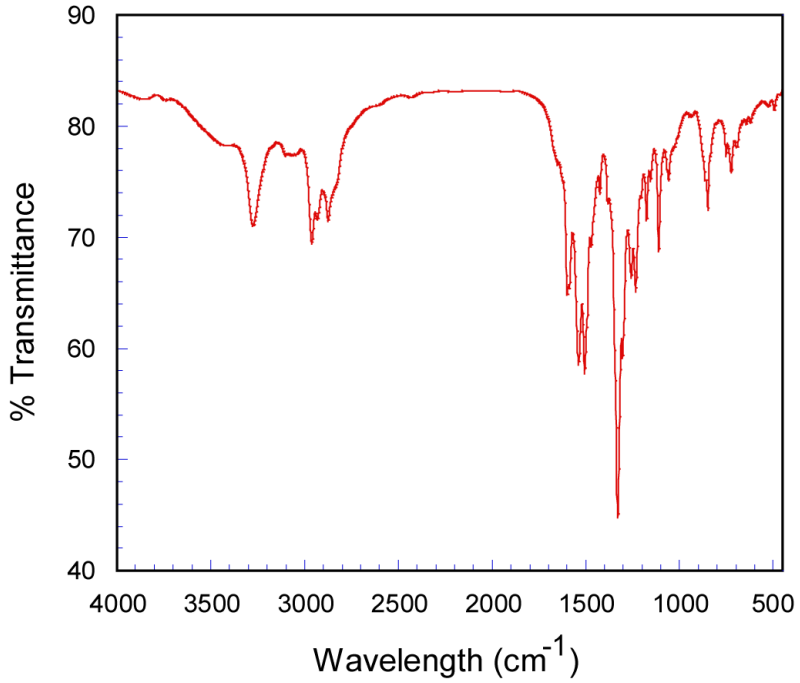

Figure S15. FT-IR spectrum of fluoride complex (**2**) recorded in KBr pellet.

Anion binding study by ^{1}H NMR titration experiments:

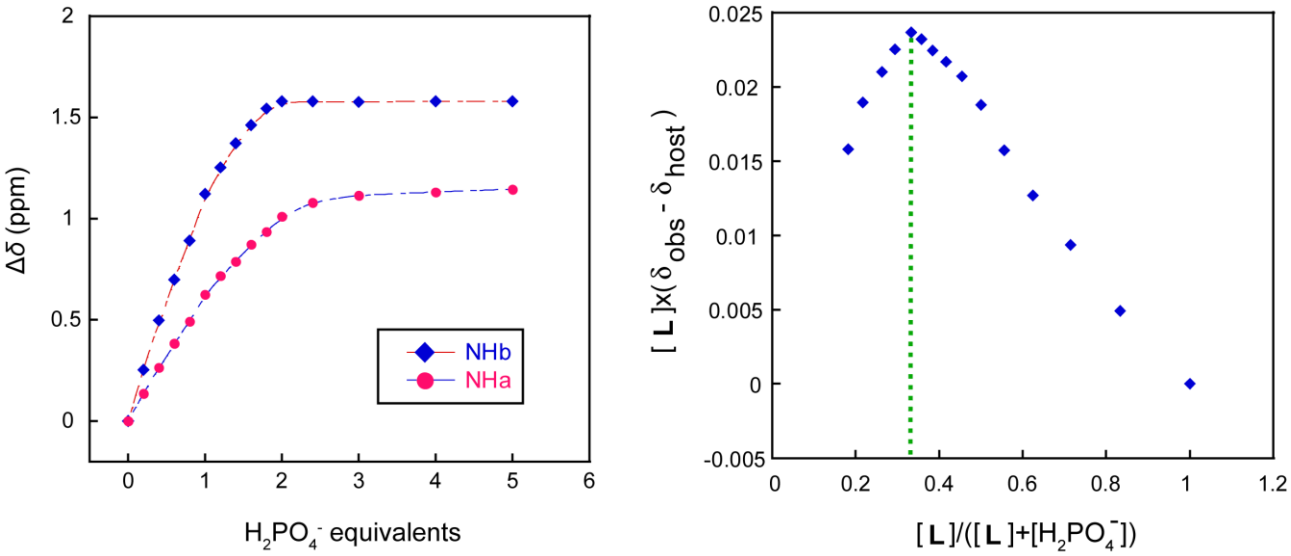

Figure S16. Change in chemical shift of –NH resonances of **L** (10 mM) with increasing conc. of standard $H_2PO_4^-$ solution (50 mM) in DMSO-d_6 at 298 K and the corresponding Job's plot suggesting the formation of 1:2 host/guest complexes in solution.

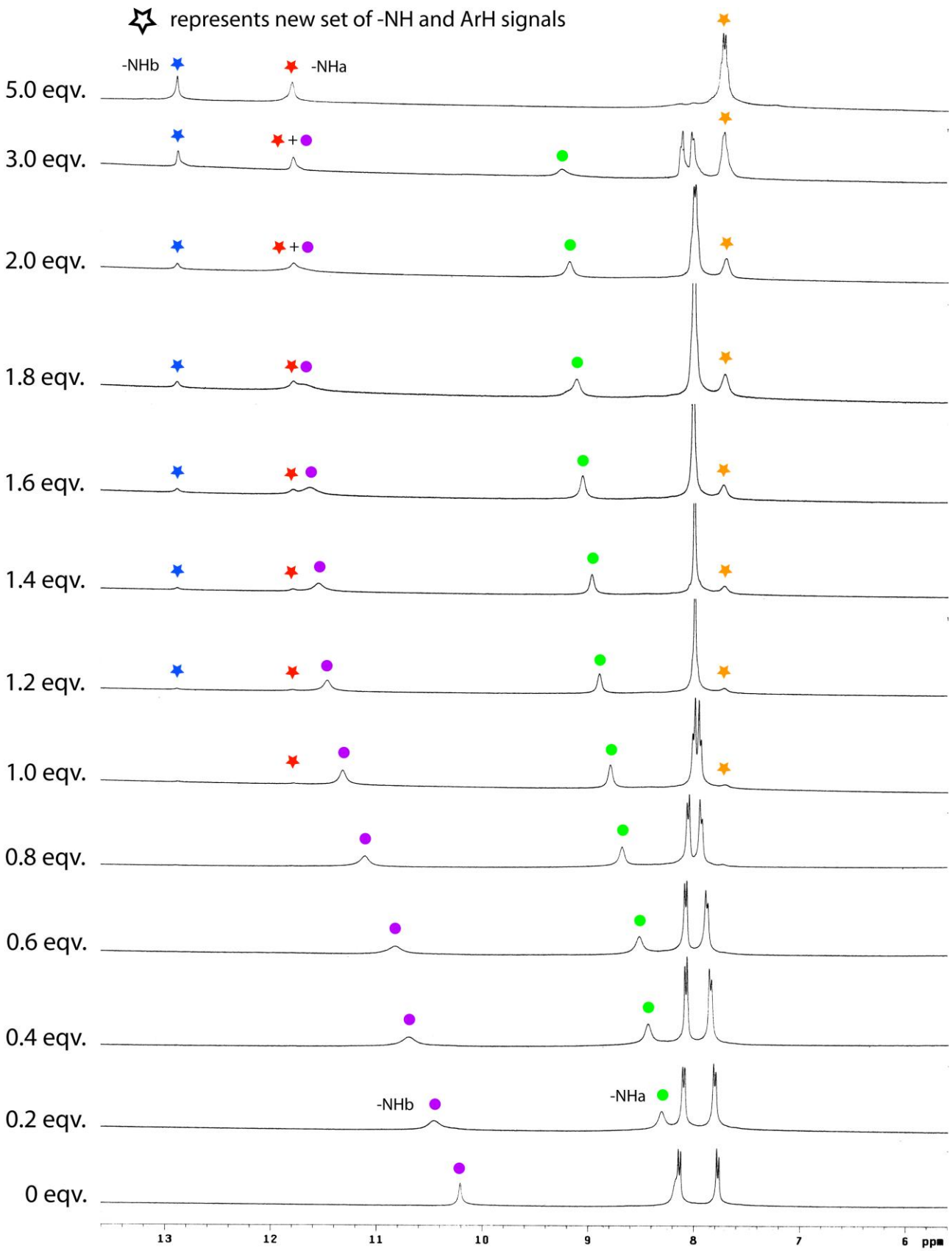

Figure S17. Expanded ^{1}H NMR spectra of **L** upon titration with $H_2PO_4^-$ ions in DMSO-d_6.

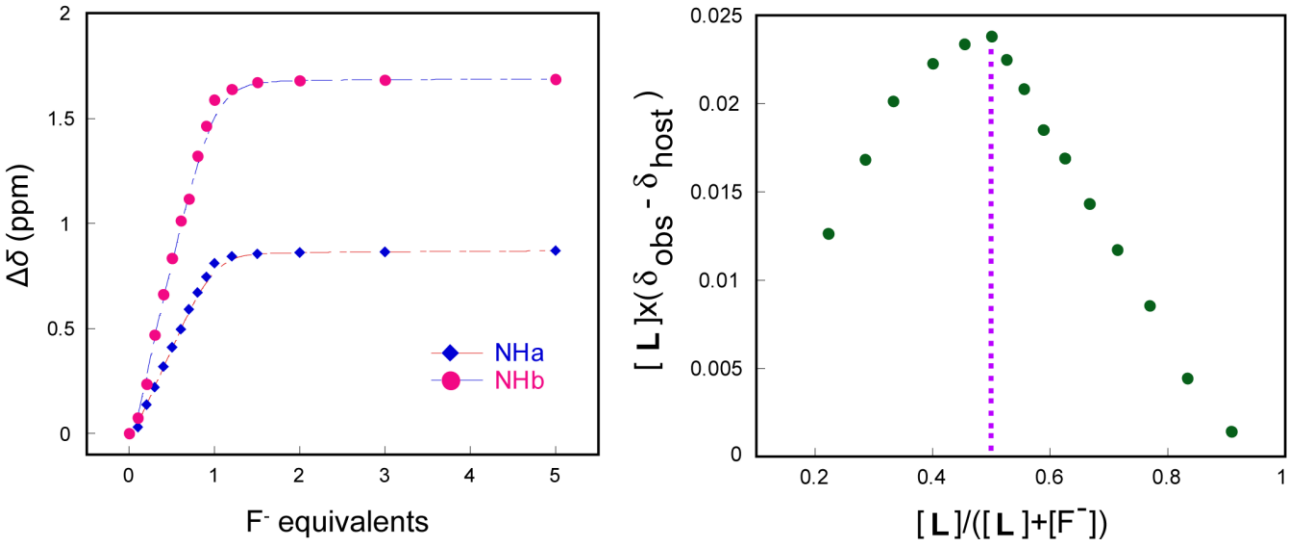

Figure S18. Change in chemical shift of –NH resonances of **L** (10 mM) with increasing conc. of standard F^- solution (50 mM) in DMSO-d_6 at 298 K and the corresponding Job's plot.

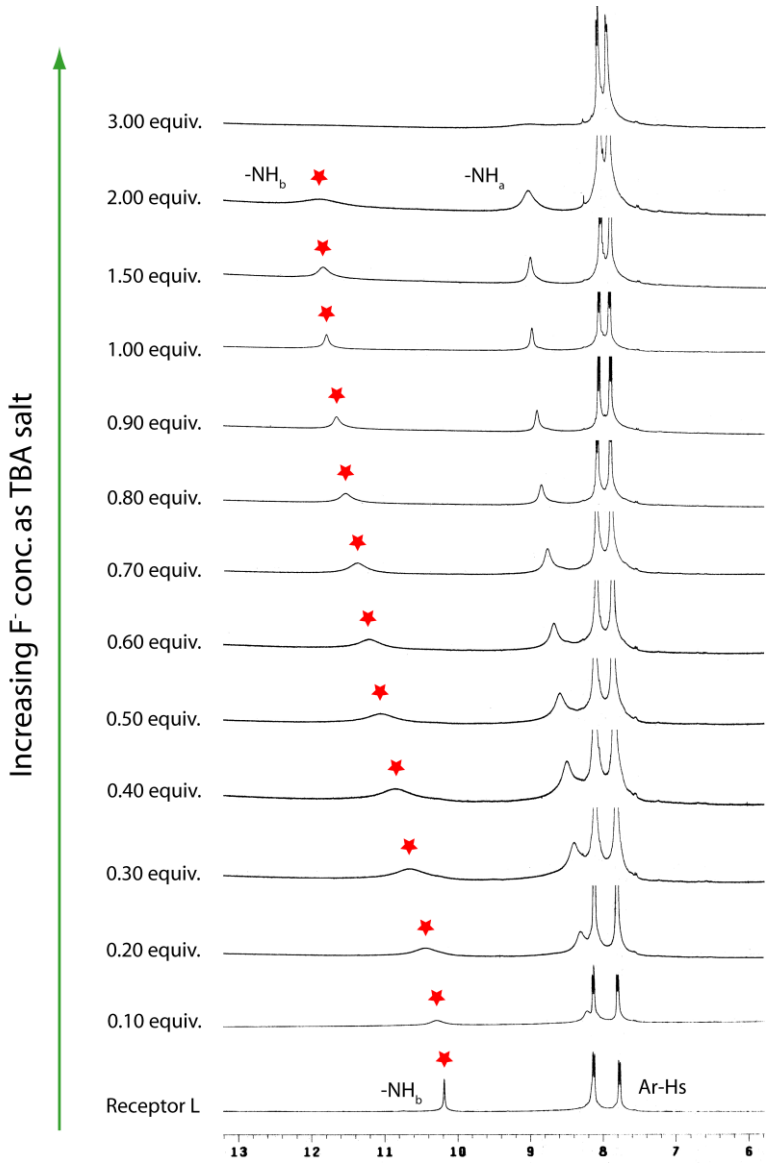

Figure S19. Expanded ^{1}H NMR spectra of **L** upon gradual addition of TBAF in DMSO-d_6.

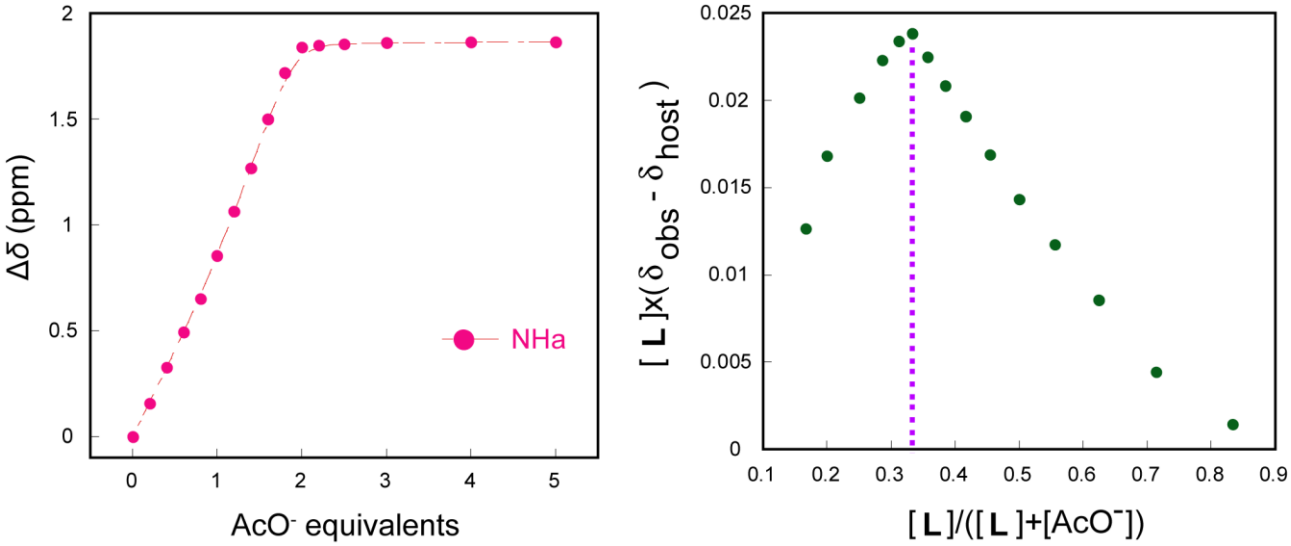

Figure S20. Change in chemical shift of –NH resonances of **L** (10 mM) with increasing conc. of standard AcO^- solution (50 mM) in DMSO-d_6 at 298 K and the corresponding Job's plot.

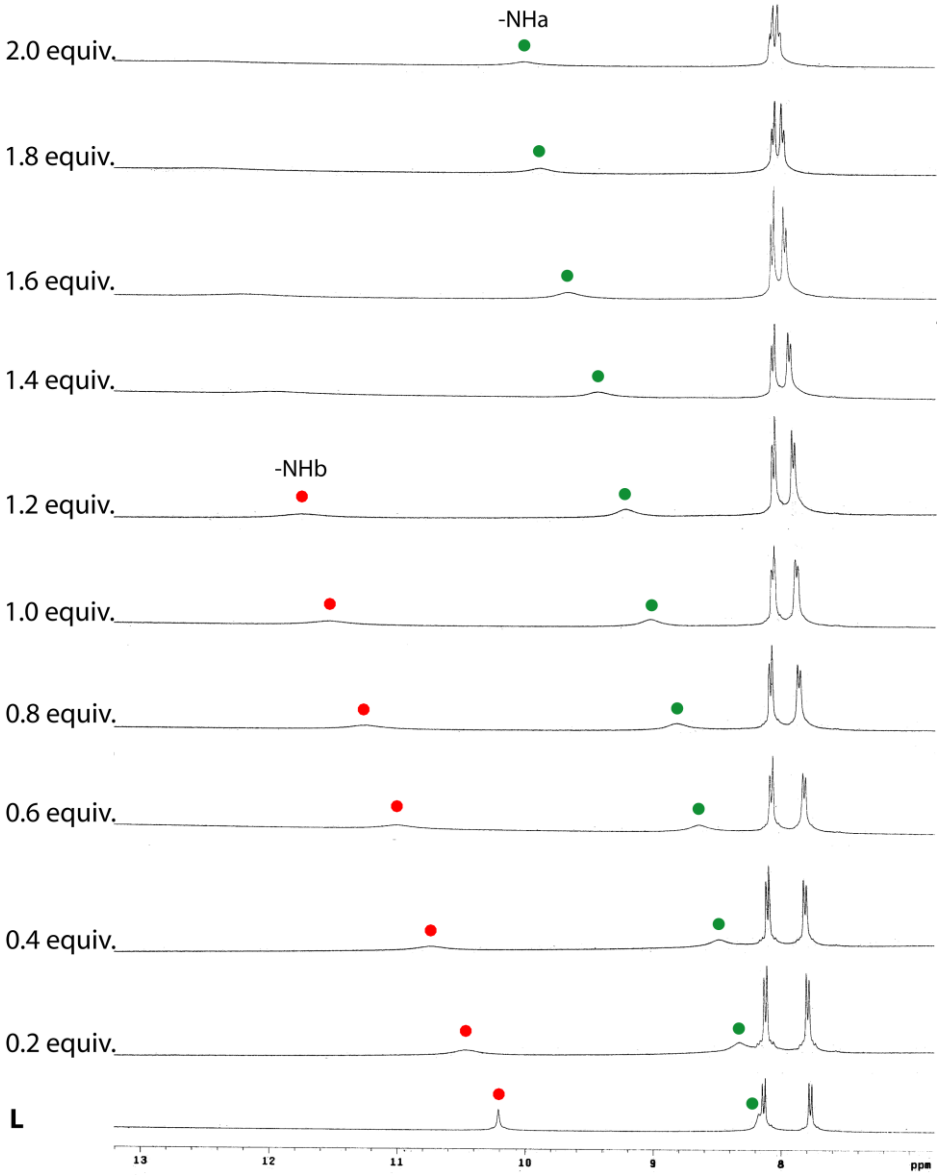

Figure S21. Expanded ^{1}H NMR spectra of **L** upon titration with AcO^- ions in DMSO-d_6.

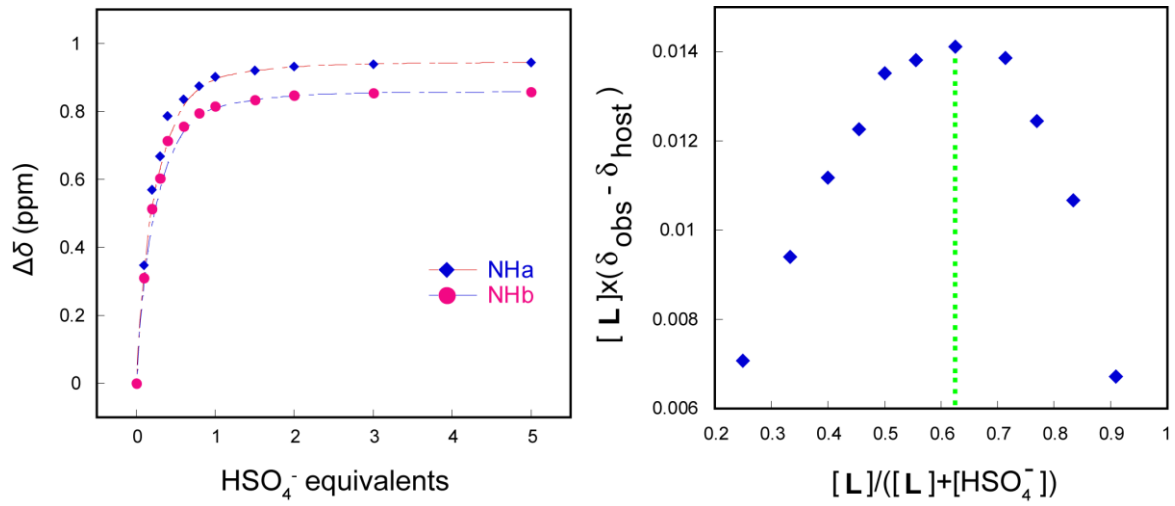

Figure S22. Change in chemical shift of –NH resonances of **L** (10 mM) with increasing concentration of standard HSO_4^- solution (50 mM) in DMSO-d_6 at 298 K and the corresponding Job's plot.

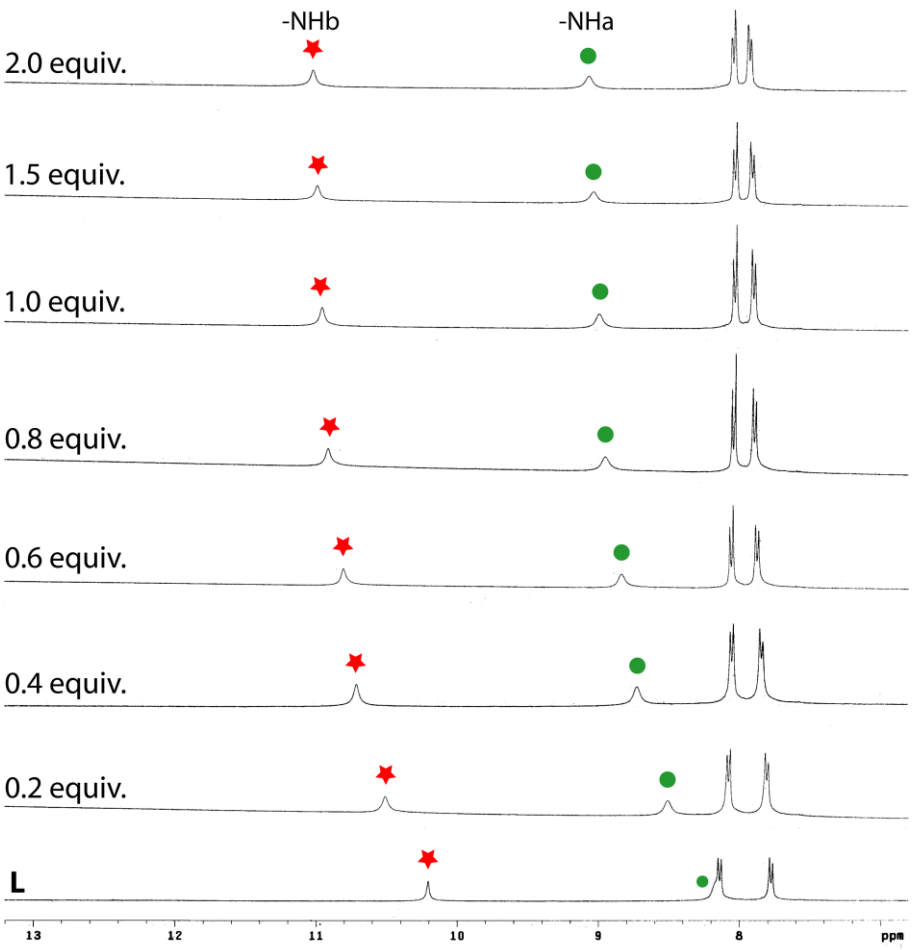

Figure S23. Expanded ^{1}H NMR spectra of **L** upon titration with HSO_4^- ions in DMSO-d_6.

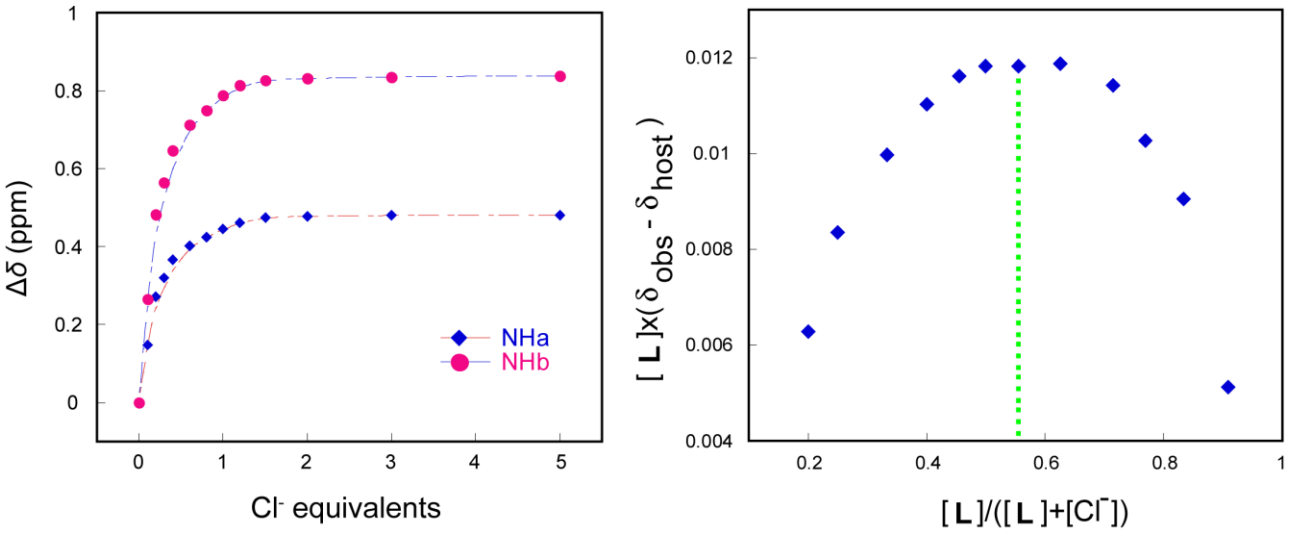

Figure S24. Change in chemical shift of –NH resonances of **L** (10 mM) with increasing concentration of standard Cl^- solution (50 mM) in DMSO-d_6 at 298 K and the corresponding Job's plot.

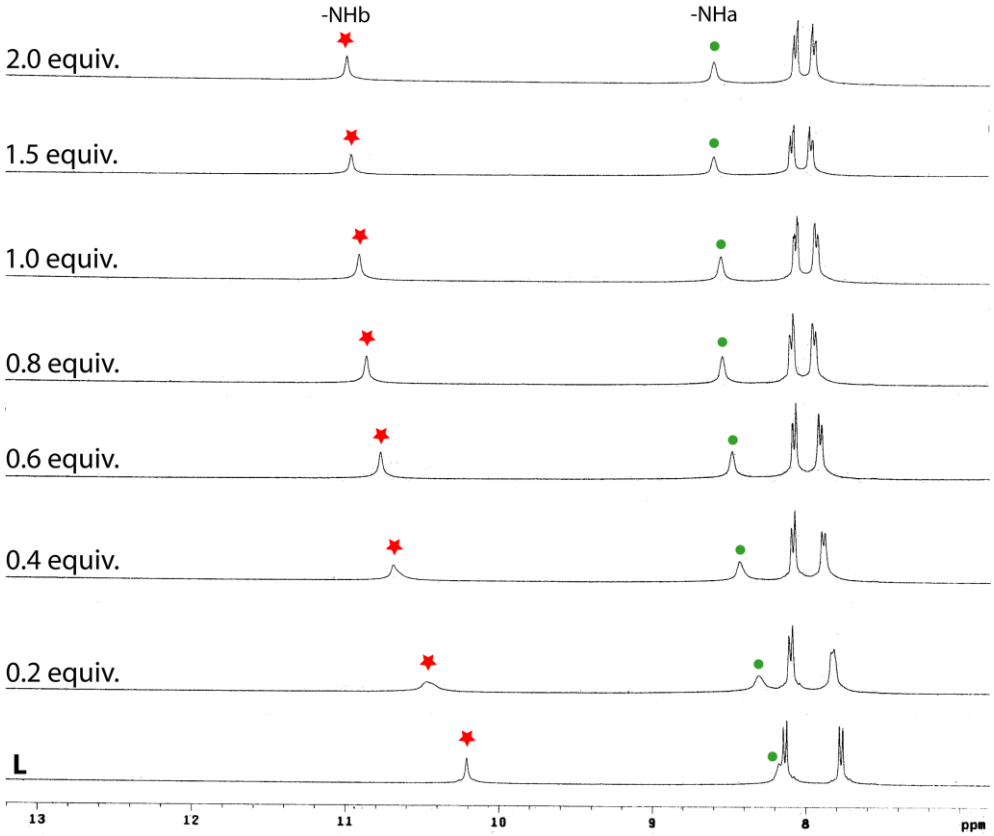

Figure S25. Expanded ^{1}H NMR spectra of **L** upon gradual addition of Cl^- ions in DMSO-d_6.

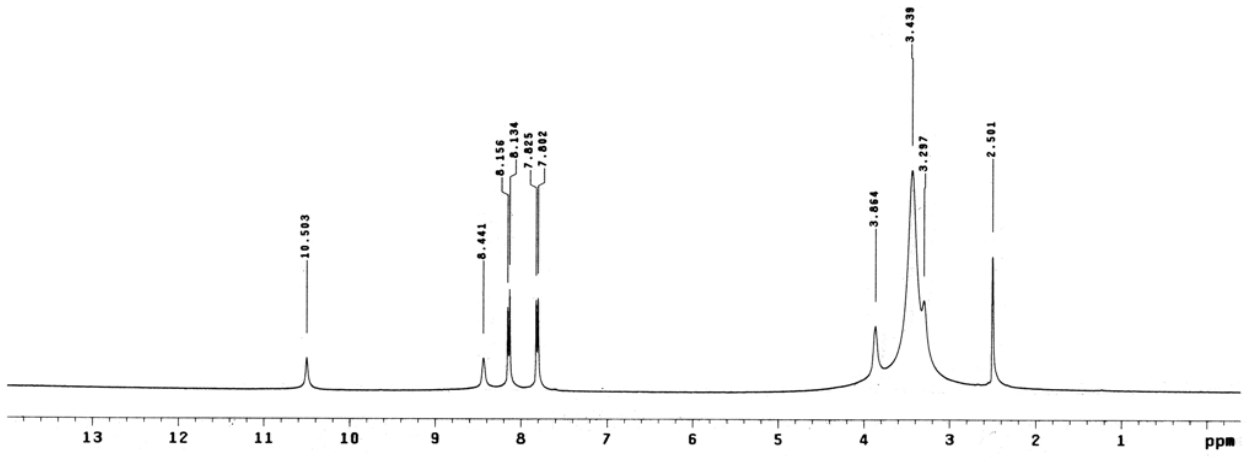

Figure S26. ^{1}H NMR spectrum of isolated salt of **L** with orthophosphoric acid (H_3PO_4).

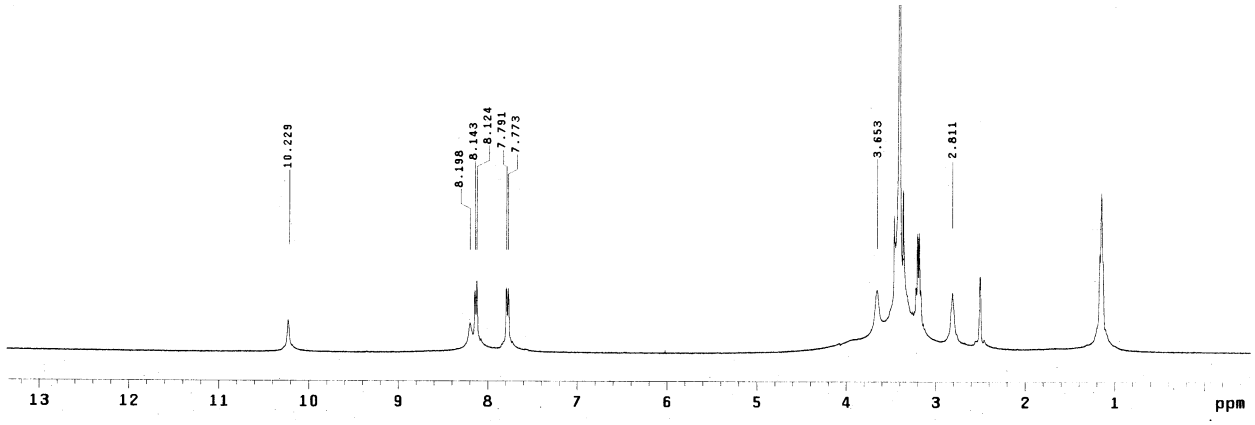

Figure S27. ^{1}H NMR spectrum of **L** in presence of tetraethyl ammonium nitrate.

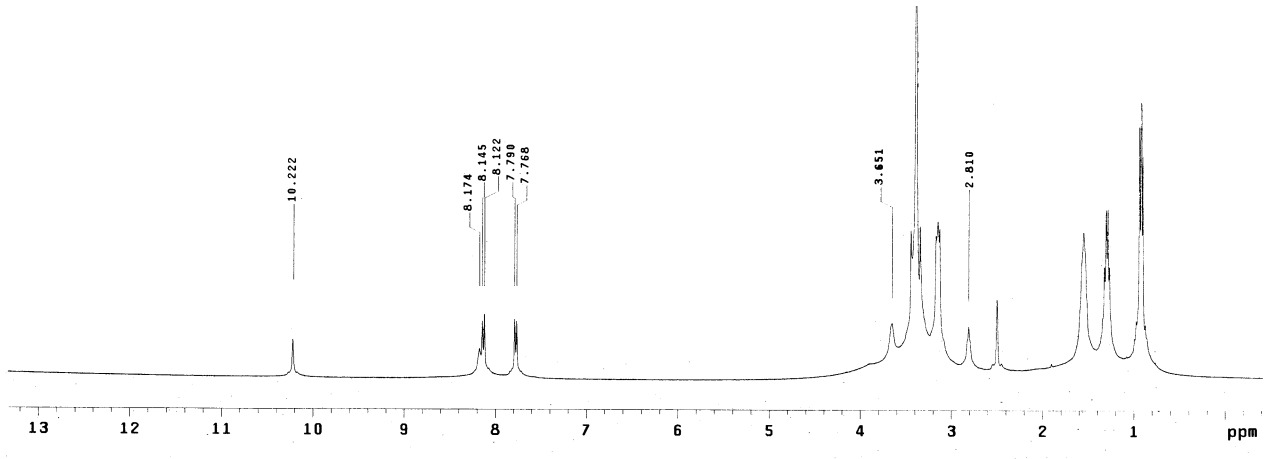

Figure S28. ^{1}H NMR spectrum of **L** in presence of tetrabutylammonium perchlorate.

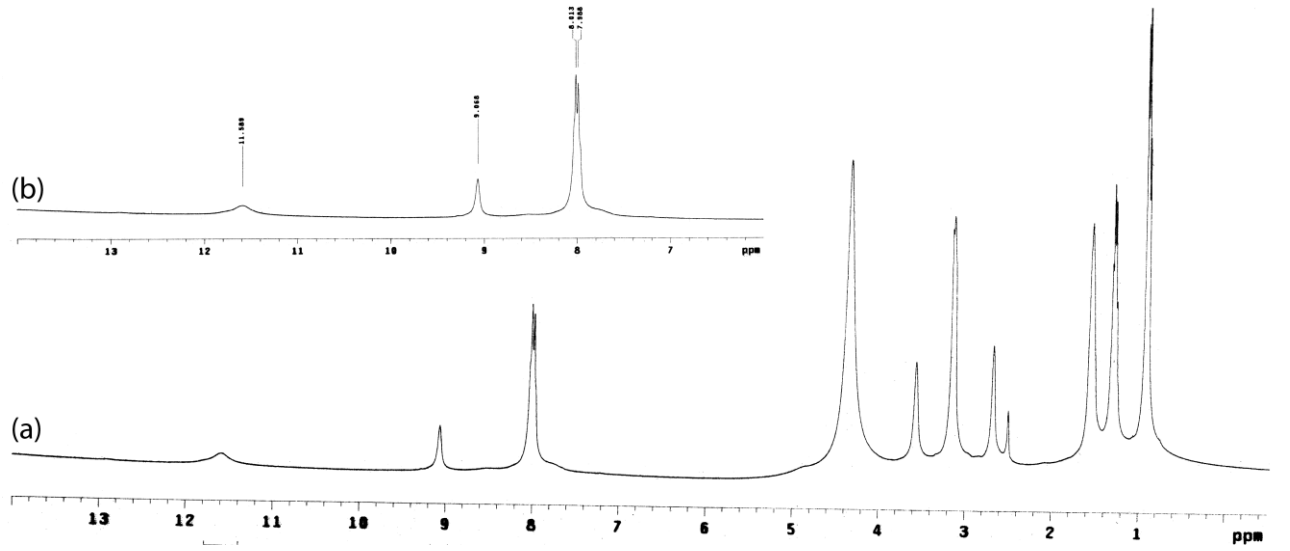

Figure S29. (a) ^{1}H NMR spectrum of **L** in presence of 1 equivalent of tetrabutylammonium $H_2PO_4^-$ recorded after overnight equilibration in DMSO-d_6; (b) Partial ^{1}H NMR spectrum (aromatic region) shows that, PO_4^{3-} complex (**1**) does not form at equivalent stoichiometry of $H_2PO_4^-$.

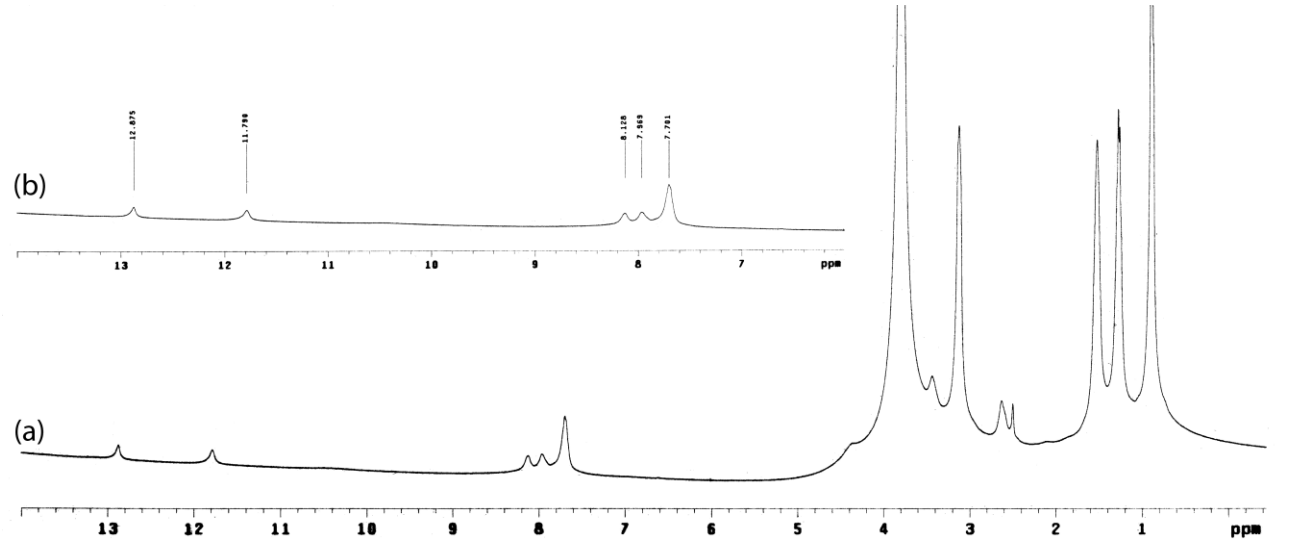

Figure S30. (a) ^{1}H NMR spectrum of **L** in presence of 3 equivalent of tetrabutylammonium dihydrogenphosphate recorded after overnight equilibration in DMSO-d_6; (b) Partial ^{1}H NMR spectrum (aromatic region) shows insitu generation of PO_4^{3-} complex (**1**) in greater percentage than the complex formed between added $H_2PO_4^-$ and **L.**

References:

1. I. Ravikumar, P. S. Lakshminarayanan, M. Arunachalam, E. Suresh and P. Ghosh, Dalton Trans., 2009, 4160–4168.